Stain Color Adaptive Normalization (SCAN) algorithm: Separation and standardization of histological stains in digital pathology

Computer Methods and Programs in Biomedicine 193 (2020) 105506

Contents lists available at ScienceDirect

Computer Methods and Programs in Biomedicine

journal homepage: www.elsevier.com/locate/cmpb

Stain Color Adaptive Normalization (SCAN) algorithm: Separation and standardization of histological stains in digital pathology

Massimo Salvi*, Nicola Michielli, Filippo Molinari

Politecnico di Torino, PoliToBIOMed Lab, Biolab, Department of Electronics and Telecommunications, Corso Duca degli Abruzzi 24, 10129, Turin, Italy

ARTICLE INFO

Article history:
Received 10 March 2020
Revised 8 April 2020
Accepted 8 April 2020

Keywords:
Color deconvolution
Digital histopathology
H&E staining
Stain normalization
Whole-slide imaging

ABSTRACT

Background and objective: The diagnosis of histopathological images is based on the visual analysis of tissue slices under a light microscope. However, the histological tissue appearance may assume different color intensities depending on the staining process, operator ability and scanner specifications. This stain variability affects the diagnosis of the pathologist and decreases the accuracy of computer-aided diagnosis systems. In this context, the stain normalization process has proved to be a powerful tool to cope with this issue, allowing to standardize the stain color appearance of a source image respect to a reference image.

Methods: In this paper, novel fully automated stain separation and normalization approaches for hematoxylin and eosin stained histological slides are presented. The proposed algorithm, named SCAN (Stain Color Adaptive Normalization), is based on segmentation and clustering strategies for cellular structures detection. The SCAN algorithm is able to improve the contrast between histological tissue and background and preserve local structures without changing the color of the lumen and the background.

Results: Both stain separation and normalization techniques were qualitatively and quantitively validated on a multi-tissue and multiscale dataset, with highly satisfactory results, outperforming the state-of-the-art approaches. SCAN was also tested on whole-slide images with high performances and low computational times.

Conclusions: The potential contribution of the proposed standardization approach is twofold: the improvement of visual diagnosis in digital histopathology and the development of powerful pre-processing strategies to automated classification techniques for cancer detection.

1. Introduction

The reproducibility of the color appearance in light microscopy plays a crucial role in the analysis of histopathological images. In routine histology, different staining dyes are used to make the cellular components visible and visualize the tissue. The most common staining method is called hematoxylin and eosin (H&E) [1]. Hematoxylin is a basic dye that binds acidic structures such as cell nuclei; while eosin is an acidic and negative charged dye that enhances basic structures such as cell stroma. According to this staining method, the cell nuclei and parts of the cytoplasm that contain RNA assume a purplish blue while the rest of the cytoplasm becomes a magenta-red structure. Thanks to the selective staining of the H&E, the pathologist is able to perform the clinical diagnosis of the histological specimen. The evaluation of histological images allows the identification of specific neoplastic regions and represents the gold standard in diagnosing several types of cancer [2,3]. However, the manual and visual assessment of digital histopathological images is time-consuming and prone to errors due to inter- and intra-operator variability [4,5]. The development of automated techniques for the quantitative analysis of histopathological images can potentially alleviate shortcomings of human interpretation.

The appearance of histological stains often suffers from large variability [6,7]. The main causes are: (i) the chemical reaction of a particular dye used in staining and the exposure time, (ii) the operator ability and (iii) the specifications of the slide scanner. In this context, the standardization of the color appearance takes on great importance both in the diagnostic field and in the development of automated solutions for quantitative analysis of histopathological images [8,9,10]. This concept could be translated into a stain normalization method. It is based on the stain separation technique, which allows to isolate the hematoxylin and eosin channels in the histological image and then the color appearance is standardized respect to a reference image (with an optimal and reproducible staining distribution) chosen by an expert pathologist.

* Corresponding author at: Biolab, Department of Electronics and Telecommunications, Politecnico di Torino, Corso Duca degli Abruzzi, 24 - 10129 Torino, Italy.
E-mail address: massimo.salvi@polito.it (M. Salvi).

https://doi.org/10.1016/j.cmpb.2020.105506
0169-2607/

The stain normalization technique could be employed both to improve the visual diagnosis of the pathologist and to increase the performance of automated classification systems. In fact, the normalization of the hematoxylin and eosin channels could be a useful pre-processing strategy to deep learning algorithm to improve the segmentation and classification performances with the aim to help pathologists in their routine work.

In this paper, a novel adaptive stain separation strategy and a structure-based stain normalization method for histopathological H&E images is presented. The proposed algorithm, named SCAN (Stain Color Adaptive Normalization), is able to improve the contrast between histological tissue and background and preserve local structures without changing the color of the lumen and the background. Our approach outperforms the state-of-the-art methods in normalizing histological slides [11–16] with lower or comparable computational times. The comparison with competing techniques was carried out both for the stain separation and normalization. To the best of our knowledge, this is the first work in which the estimation of stain vectors was quantitatively assessed, in addition to stain normalization performance comparison. The quantitative metrics were computed by using a ground truth obtained with the help of an expert pathologist (20 years of experience), which manually selected the areas with a pure stain of hematoxylin and eosin. The SCAN algorithm was validated on a multi-tissue and multiscale dataset of H&E stained tissue images. In addition, the method was also tested on whole-slide images (WSIs) with highly satisfactory results.

The remainder of this paper is organized as follows. In Section 2 an overview of the background and a description of the state-of-the-art methods are presented. An exhaustive description of the proposed approach is provided in Section 3. The experimental results are reported in Section 4 and discussed in Section 5.

2. Related work

In this section, we describe the theoretical background about the color deconvolution technique and the state-of-the-art methods for stain standardization. The aim of the color deconvolution is to isolate the contributions of the individual dyes used during the staining process. In this work, the histological slides were stained with H&E, hence the number of stains was equals to 2 (i.e. hematoxylin binds cell nuclei with a deep blue-purple color while eosin stains stroma with a pinkish color). The color intensity assumed by the specific cell component depends on the absorption of the amount of stain, according to the Beer–Lambert law [17]. The (decadic) absorbance A of a medium is defined as the common logarithm of the ratio of incident (I_0) to transmitted (I) light intensity and can be also expressed as the product of the path length l of the light beam, the molar extinction coefficient ε and the concentration c of the absorbing species:

$$A = -\log_{10}\left(\frac{I}{I_0}\right) = \varepsilon \cdot c \cdot l \tag{1}$$

The input image was vectorized in order to obtain a matrix $I \in R^{3\times N}$ where each row contained all the pixels (N) which belonged to a single RGB channel. The incident light intensity I_0 was set to 255 for 8-bit images. Let $H \in R^{r\times N}$ be the stain density map, where the rows represent the concentration of each stain (r: number of stains) and $W \in R^{3\times r}$ be the stain color appearance matrix whose columns (also called stain vectors) represent the RGB triplets for each stain converted in the optical density (OD) space using Eq. (1). The OD represents the optical attenuation, which in general includes absorption, scattering and reflection, normalized to the optical path length. In histology, hematoxylin and eosin are light-absorbing stains differently than other polymers, such as diaminobenzidine (DAB) which scatters light source [18,19]. The concept of OD could be adopted for the analysis of H&E stained histological images, considering that thickness of the sample is the same for each histological slice and the main information is the amount of stain absorbed by specific cell components in the tissue section.

The RGB intensity values cannot be directly used for stain separation since the relationship between the light intensity and the concentration of stains is nonlinear. According to Eq. (1), the corresponding OD value of each pixel for each channel is linear with the concentration of absorbing species [20], thus the OD space can be used for the separation of the contribution of each stain. Let V be the OD of the image I, expressed as the product of the stain color appearance matrix and the stain density map:

$$V = W \cdot H \tag{2}$$

Therefore, the first step of stain separation is the estimation of the matrices W and H involved in the factorization of the input RGB image in OD space. For this application, a color deconvolution was applied to isolate the structures stained with hematoxylin (nuclei) and eosin (stroma). This method allows to split an input RGB image into two separate channels related to the intensity of a particular stain concentration. Two channels are obtained from the H&E stained histological image, as described as follows:

$$V_j = W(:, j) \cdot H(j, :), \quad j = 1, 2 \tag{3}$$

where V_1 and V_2 represent the output RGB hematoxylin and eosin channel, respectively. Then, these matrices were projected into RGB color space by inverting the Beer–Lambert law:

$$I_j = I_0 \cdot 10^{-V_j}, \quad j = 1, 2 \tag{4}$$

The aim of stain separation is to factorize one input matrix into the product of two unknown matrices. In the last years, several methods were proposed with the purpose of estimating the stain color appearance matrix W. After estimating this matrix, the stain density map H can be solved by inverting the Eq. (2) and computing the Moore–Penrose pseudoinverse matrix of the non-square matrix W:

$$H = \left(\left(W^T \cdot W\right)^{-1} \cdot W^T\right) \cdot V \tag{5}$$

After this step, all the negative elements of matrix H were set to zero, since the molar concentration of a specific stain cannot assume negative values. In this work, we solved this problem by introducing a novel definition of matrix H (as we explain in Section 3.5) without negative values, which are referred to invalid biological absorption of light by cellular structures. The stain normalization process is performed by combining the information of stain color appearance matrix and stain density map of a source image with the corresponding values of a target image. The source is the input image which presents a color appearance of difficult interpretation, while the target is a template image selected by an expert pathologist, with an optimal and reproducible staining distribution.

Based on the technique employed to normalize the H&E image, the current stain normalization methods can be grouped into three categories: color deconvolution-based, histogram transformation-based and iterative optimization-based methods.

2.1. Color deconvolution-based methods

Ruifrok et al. [20] proposed a simple algorithm to perform color deconvolution by estimating the matrix W through fixed RGB triplets for hematoxylin and eosin. Therefore, this algorithm results in a non-adaptive approach since the color variability between different histological slides is not retained and the approximate estimation of the stain vectors significantly worsens the performance

of the color deconvolution. Macenko et al. [11] proposed a method based on the singular value decomposition (SVD) with the aim of finding a plane onto which project the OD transformed pixels and finding the extreme values that correspond to the stain vectors. The advantages of this approach are its applicability to other histological stains and low computational times. The major limitation of this technique is represented by the wrong estimation of stain vectors if the unstained regions have an intensity (in OD space) higher than the imposed threshold (β=0.15). In addition, the presence of strong intensity variations of stained structures may cause a failure of the entire color deconvolution process. Khan et al. [13] employed a color deconvolution-based approach to obtain the stain matrix. They introduced a stain color descriptor (SCD) for the quantification of stain concentration and performed a nonlinear mapping to normalize a source image to target image color appearance. The drawback of this method is the high computational time respect to other techniques.

2.2. Histogram transformation-based methods

Reinhard et al. [12] implemented a transformation between a source and a target image in the $l\alpha\beta$ color space by computing the mean and the standard deviation for each channel. After performing the transformation, the normalized image was converted into the original RGB color space. However, during the normalization process, the uncolored regions (white) can be mapped as colored regions due to the effect of a low-pass filter.

2.3. Iterative optimization-based methods

Rabinovich et al. [14] compared the performance of two different color deconvolution methods: independent component analysis (ICA) and non-negative matrix factorization (NMF). ICA is a computational method for recovering statistically independent source signals (stain vectors). NMF is a mathematical method based on the matrix decomposition of multivariate data. The problem solved by NMF is to find two non-negative matrices W and H which minimize the functional:

$$f(W,H) = \frac{1}{2}\|V - WH\|_F^2, \ \ such\ that\ W,H \geq 0 \tag{6}$$

where V is the input matrix to decompose and the subscript F denotes the Frobenius norm which measures the error between the original matrix V and its low rank approximation [21]. In the standard NMF algorithm, W and H are initialized with non-negative random values and an iterative approach was employed to converge to a desired solution. In the work of Rabinovich et al. [14], the overall relative error (defined as the normalized squared difference between the ground truth and the estimate) for NMF is lower than ICA. Starting from the NMF cost function, Vahadane et al. [15] proposed an unsupervised approach by adding a sparseness regularization term on stain density map H. This method, also called sparse non-negative matrix factorization (SNMF), outperformed the classical NMF and the SVD-based normalization proposed by Macenko [11]. The main advantage of this method is the preservation of the biological structure information of the source image after the stain normalization process. Finally, Zheng et al. [16] proposed a novel adaptive color deconvolution (ACD) model for stain normalization of H&E slides. They solved a minimization problem through an integrated optimization in order to find the optimal stain weight matrix for the input histological image. The normalization is obtained by recombining the stain vectors of the source image with the stain color appearance matrix of a target. The main limitation of this work is the quantitative metric chosen to validate the method. The authors computed the normalized median intensity (NMI) which is a measure of color constancy and uniformity, but it contains no information about the similarity of the color appearance with the target image.

Table 1
Dataset composition.

Tissue	Magnifications	#Images
Adrenal	10x, 20x	50
Breast	10x, 20x	50
Colon	20x, 40x	40
Liver	10x, 20x, 40x	60
Prostate	10x, 20x	70

3. Materials and methods

In this paper, an automatic and adaptive method for color normalization of H&E stained images is presented. The flowchart of the proposed normalization is shown in Fig. 1. The SCAN algorithm consists of four modules: preliminary stain separation, cellular structures segmentation, final stain separation and image normalization. The proposed method is based on an adaptive refinement of the SVD-based approach proposed by Macenko et al. [11] using segmentation and clustering strategies for nuclei and stroma detection. The stain density map was then estimated trying to maintain its physical meaning according to Beer–Lambert law. In the following sections, a detailed description of the algorithm is provided.

3.1. Image dataset

Our dataset consisted of 270 H&E stained tissue images taken from five organs (adrenal gland, breast, colon, liver, prostate) and three magnifications (10x, 20x, 40x). Each image had a fixed dimension of 1024 × 2048 pixels. The overall dataset composition is shown in Table 1. The image dataset, along with the manual annotations, are available at https://data.mendeley.com/datasets/sc878z8pm3/1.

3.2. Preliminary stain estimation

Starting from the original RGB image of the specimen, SCAN performed a white detection in order to exclude from the processing all the uncolored regions (e.g. background, gland lumen, etc.).

Simple thresholding may be ineffective to detect all white regions since they often have different intensity depending on their size, shape and presence of artifacts. Therefore, in order to properly segment all these regions, a series of Gabor kernels was applied to the original grayscale image. The kernels are defined as follows:

$$g(x,y,\lambda,\theta,\ \ \psi,\sigma,\gamma) = \exp\left(-\frac{x'^2+\gamma^2 y'^2}{2\sigma^2}\right)\cos\left(\frac{2\pi x'}{\lambda}+\ \ \psi\right) \tag{7}$$

where $x' = xcos(\theta)+ysin(\theta)$, $y' = -xsin(\theta)+ycos(\theta)$, γ is the spatial aspect ratio that specifies the ellipticity of the Gabor function, ψ represents the phase offset, λ is the wavelength of the sinusoidal factor, θ denotes the orientation of the normal to the parallel stripes of a Gabor function and σ is the standard deviation of the Gaussian envelope [22]. For this application, we imposed $\gamma = 1.2$, $\psi = 0$, $\lambda = 10$, $\sigma = 1$ and eight directions (θ) were considered to make the algorithm faster and to still reduce the noise level. The obtained eight filtered images were summed and normalized; then a threshold equal to 90% of the image maximum was applied (Fig. 1a).

All detected white regions were removed with the aim to process only the H&E stained structures. Then, color deconvolution proposed by Macenko et al. [11] was applied to obtain the first separation between hematoxylin and eosin channels (Fig. 1b).

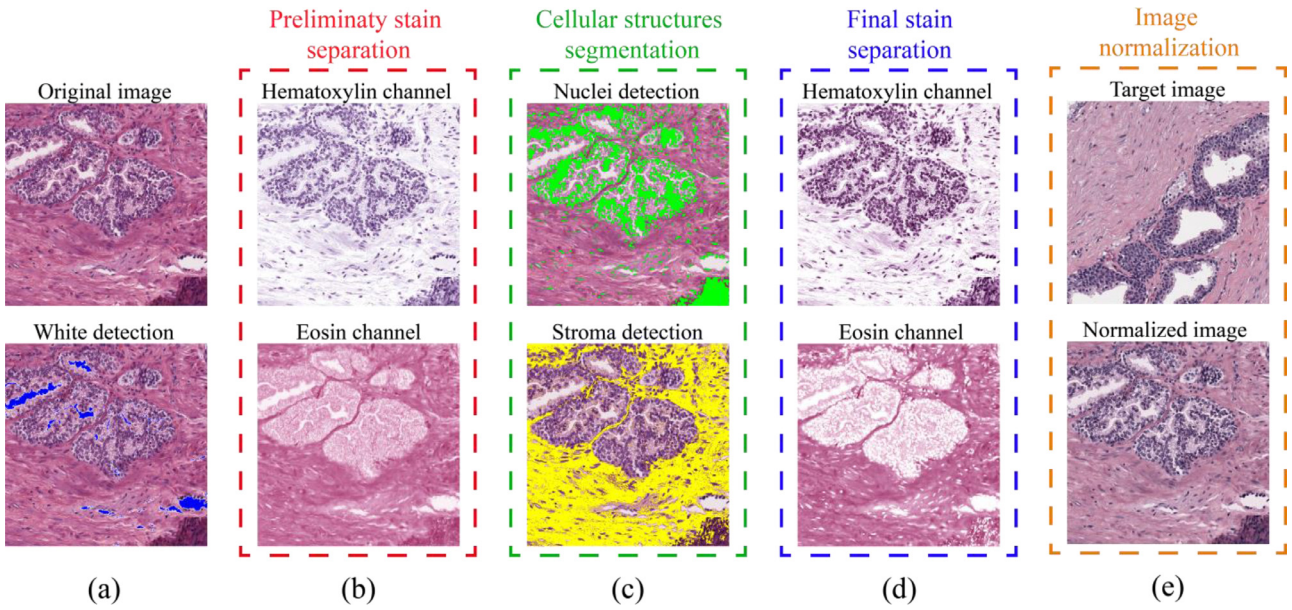

Fig. 1. Flowchart of the SCAN algorithm. (a) original image and white detection (in blue), (b) preliminary stain separation using SVD-geodesic method [11], (c) cellular structure segmentation, (d) final stain separation, (e) image normalization.

3.3. Cellular structures segmentation

The next step of the SCAN algorithm is the segmentation of the cellular regions of interest: nuclei (hematoxylin) and stroma (eosin). Firstly, the hematoxylin channel was intensity normalized and then Wiener filtered, in order to smooth the intensity of the nuclei. The obtained image is thresholded using an improved version of the MANA algorithm [23]. Thresholding was firstly performed by computing the probability p of each gray value in the filtered image, then dividing the image histogram into 128 bins to obtain a number of thresholding points $T = (\frac{256}{bins}) \cdot k$, where k indicates the kth bin. For each thresholding point, p_0 represents the probability of having gray values equal or lower than T while p_1 is defined as $1 - p_0$. Hence, p_0 and p_1 are related to the background and nuclei distribution, respectively. Then, an energy function was computed as:

$$energy = -\left(\sigma^2 \cdot \log\left(\sigma^2\right) - p_0^2 \cdot \sigma_0^2 \cdot \log\left(\sigma_0^2\right) - p_1^2 \cdot \sigma_1^2 \cdot \log\left(\sigma_1^2\right)\right) \tag{8}$$

where σ^2 is the variance of the whole image, σ_0^2 and σ_1^2 are the variances of the probability functions of the two classes. The optimal thresholding point was then found by minimizing the energy function in Eq. (8). The result of nuclei detection is shown in Fig. 1c.

In order to identify stroma regions, a k-means clustering was applied to the image $D = Eos - Hem$, where Eos and Hem are the eosin and hematoxylin channels, respectively. Then, all negative values of D were set to zero. This channel subtraction aims to brighten the stromal response while simultaneously darkening everything belonging to nuclei or background. The fast k-means algorithm [24] was then applied with a number of clusters equal to 2: stroma and background. The initial centroids for clustering were respectively the pixel with the highest and lowest intensity within image D. Finally, stroma pixels were defined as the pixels belonging to the cluster with the higher mean intensity (Fig. 1c).

3.4. Final stain separation

Starting from the segmentation masks of the previous step, the SCAN algorithm computed the median RGB values of nuclei and stroma within the image. Then, RGB values were converted into OD space and compared with the ones obtained with the preliminary stain separation. A new color deconvolution was defined by considering the OD stains extracted from the segmentation masks. This process was repeated until the difference between the old and new OD stains was higher than 0.10. Finally, the stain color appearance matrix W was normalized in order to have stain vectors with unit Euclidean norm [20]. The final stain separation is provided in Fig. 1d.

3.5. Stain normalization

In order to normalize the image, the stain density map H should also be estimated. Several state-of-the-art works [20,11,13] computed this unknown matrix by inverting the non-square matrix W using Eq. (5), but this approach does not maintain the physical meaning of the stain density map. In fact, the numerical inversion could introduce some errors in the concentration estimation (e.g. negative values which are not physically admitted). For this reason, we computed the first row $H(1, :)$ as the median of RGB triplets deriving from the first channel of color deconvolution (hematoxylin estimation) normalized by the first stain vector $W(:, 1)$. This process was repeated equivalently for the second row of H using the second deconvolved channel (eosin estimation). This scaled version of stain density map was computed both for source and target image, obtaining H_S and H_T, respectively. Then, the normalized stain density map of the source image (H_s^{norm}) was obtained using the following equation:

$$H_s^{norm}(j, :) = \frac{H_s(j, :)}{H_s^{RM}(j)} H_T^{RM}(j), \quad j = 1, 2 \tag{9}$$

where the superscript RM denotes the robust pseudo maximum of each row vector at 99% and j indicates the stain analyzed (first row: hematoxylin, second row: eosin). Finally, the normalized source image (I_s^{norm}) was obtained using the following transforma-

Table 2
Quantitative comparisons (rSE) for different stain separation methods. rSE_{HEM} and rSE_{EOS} indicate the rSE of stain estimation for the hematoxylin and eosin, respectively.

Tissue	Macenko et al. [11]		Khan et al. [13]		Rabinovich et al. [14]		Vahadane et al. [15]		SCAN algorithm	
	rSE_{HEM}	rSE_{EOS}	rSE_{HEM}	rSE_{EOS}	rSE_{HEM}	rSE_{EOS}	rSE_{HEM}	rSE_{EOS}	rSE_{HEM}	rSE_{EOS}
Adrenal	0.0119	0.0086	0.0015	0.0042	0.0083	0.0129	0.0031	0.0027	**0.0008**	**0.0009**
Breast	0.0086	0.0172	0.0009	0.0154	0.0053	0.0026	0.0013	0.0036	**0.0005**	**0.0025**
Colon	0.0094	0.0071	0.0022	0.0022	0.0041	0.0086	0.0014	0.0023	**0.0009**	**0.0011**
Liver	0.0088	0.0053	0.0030	**0.0005**	0.0066	0.0119	0.0024	0.0045	**0.0005**	0.0010
Prostate	0.0061	0.0097	0.0051	0.0032	0.0033	0.0062	0.0012	0.0017	**0.0010**	**0.0007**

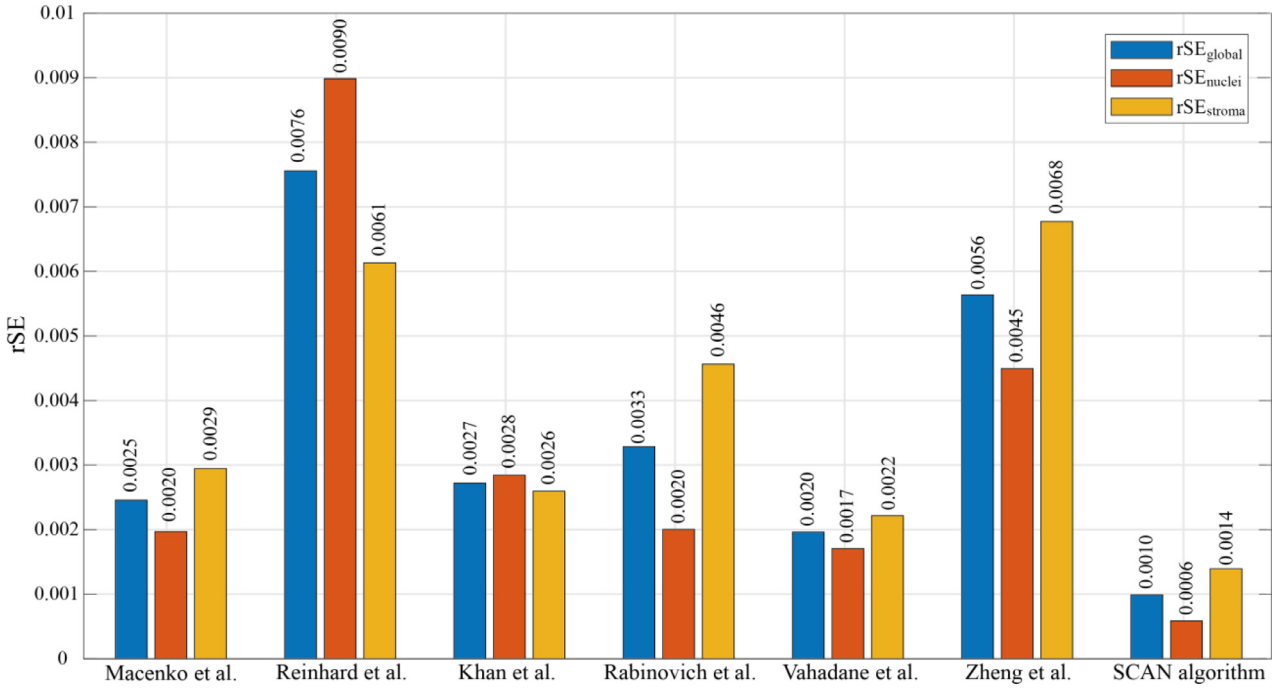

Fig. 2. Quantitative comparison between the SCAN algorithm and the state-of-the-art methods during stain normalization. rSE_{global} indicates the relative square error made for the whole image while rSE_{nuclei} and rSE_{stroma} represent the errors for the nuclei and stroma, respectively.

tion [15]:

$$V_s^{norm} = W_T \cdot H_s^{norm} \tag{10}$$

$$I_s^{norm} = I_0 \cdot 10^{(-V_s^{norm})} \tag{11}$$

where W_T is the target stain color appearance matrix and V_s^{norm} denotes the normalized source image in optical density space. In this way, once accurate stain separation was done, our color normalization technique only changed the stain color appearance while preserving the source structures. The result of this process is reported in Fig. 1e. To the best of our knowledge, SCAN is the first stain separation and normalization method developed to detect the true stain intensities through cellular structures segmentation.

3.6. Performance measures

The proposed method was compared with other state-of-the-art approaches for both stain separation and normalization. An expert pathologist (20 years of experience) generated the ground truth used for quantitative comparison. Specifically, the specialist manually annotated regions of different pure stains and the median value was extracted to assembly the ground truth stain color appearance matrix W_{GT}. Then, the relative Square Error (rSE) was computed as follows:

$$rSE = \frac{\|(W - W_{GT})^T (W - W_{GT})\|}{\sqrt{\|(W)^T (W)\| \cdot \|(W_{GT})^T (W_{GT})\|}} = \frac{\|W - W_{GT}\|_F^2}{\|W\|_F \cdot \|W_{GT}\|_F} \tag{12}$$

where $\|\cdot\|$ denotes the matrix trace and the subscript F indicates the Frobenius norm of the matrix. This metric assesses the ability of an automated method to estimate stain vectors close to ground truth ones and it is useful to quantitatively asses the consistency of the stain normalization. The lower the rSE, the better the performance of the method. This error was computed to evaluate both the performances of stain separation and normalization process. To assess the stain separation performance, the rSE was calculated between the stain matrix of the original image (W_{GT}) and the estimated color appearance matrix (W) at the end of the stain separation process. In this case, the rSE measure could be computed by considering only the first/second column of the stain color appearance matrix to evaluate the stain estimation error (rSE_{HEM}, rSE_{EOS}) for hematoxylin and eosin, respectively. This metric was also used to assess the quality of the stain normalization process by calculating the rSE using the stain color appearance of the target and the stain matrix of the normalized image as W_{GT} and W, respectively. In this way, the rSE could be evaluated for the whole normalized image (rSE_{global}) or for the two types of cellular structures (nuclei, stroma) within the normalized image.

In the last few years, several metrics have been proposed to evaluate the performance of a stain normalization method (e.g. multichannel Pearson correlation coefficient, quaternion structural similarity index (QSSIM) [15] and NMI [16]). Among these, Pearson coefficient and QSSIM can be computed only when the target image is the same version of the source image but acquired with a

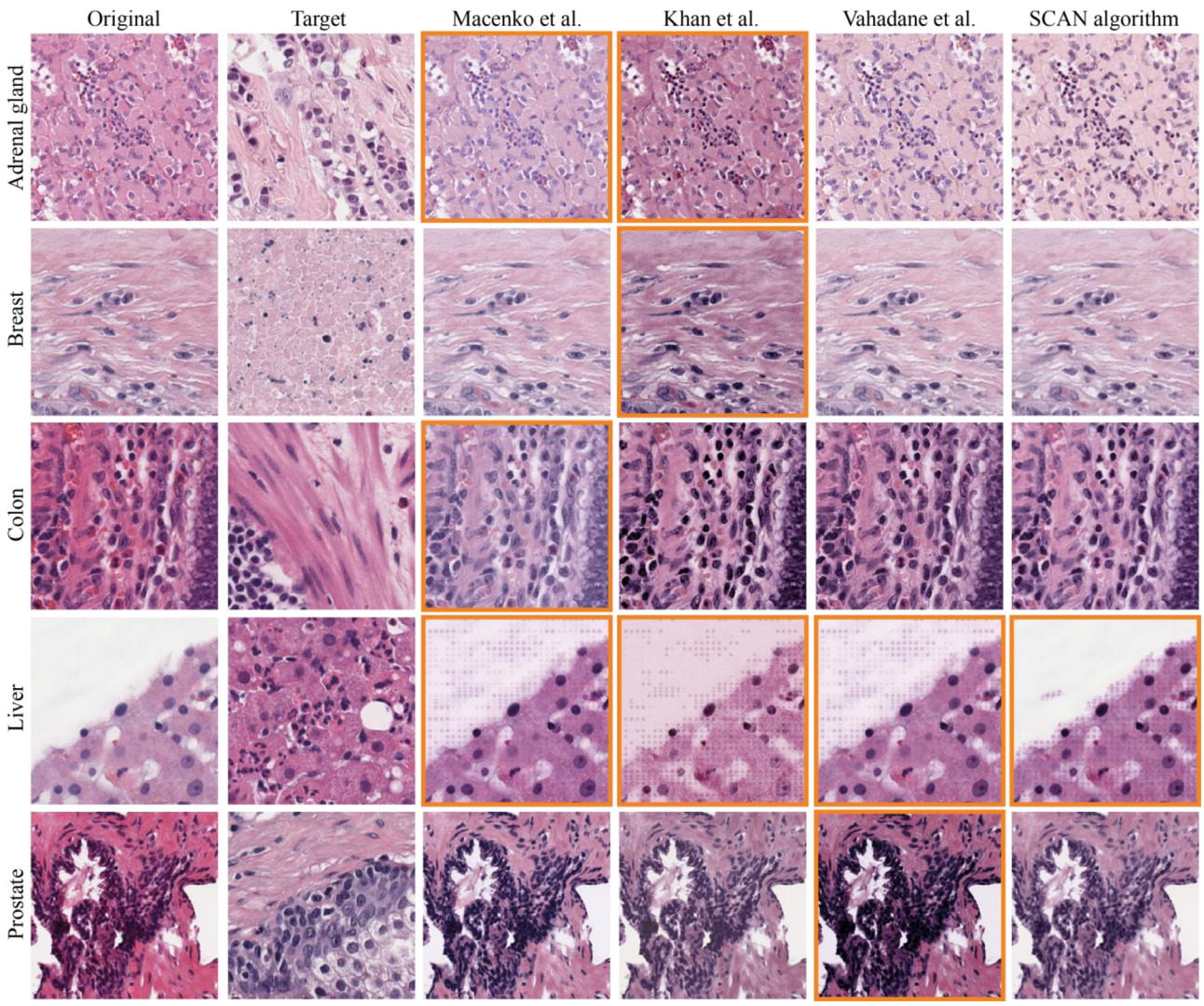

Fig. 3. Visual performance between the best three published methods for stain normalization and the proposed algorithm. Sub-images from different tissues are shown in rows while color normalization results are illustrated in columns. First column displays the original ROI while the second one illustrates the target image. Compared methods are presented from the third column while SCAN algorithm is shown in the last one. Results that have apparent artifacts are framed with orange boxes.

different scanner. On the other hand, the NMI measure is able only to quantify the intensity degradation and it retains no information related to target color appearance. For these reasons, the rSE proposed by Vahadane et al. [15] can be considered a more robust metric to quantitatively assess the similarity of the normalized image to the target one.

4. Results

4.1. Stain separation performance

The stain separation methods developed from different aspects of the histological images were compared. Specifically, the SVD-geodesic method proposed by Macenko et al. [11], the separate-transformation-based method proposed by Khan et al. [13], and other two unified-transformation-based methods developed by Rabinovich et al. [14] and Vahadane et al. [15] were involved in the comparison. The methodologies of these approaches are introduced in the related works (Section 2). The results of the compared methods are presented in Table 2. Our method exhibited excellent performance in the color deconvolution process, surpassing all the previously published techniques in all tissues except for the eosin component in liver, where the method proposed by Khan et al. [13] reported a better result.

4.2. Stain normalization performance

To evaluate the quality of normalization, an expert pathologist chose a target image for each of the five tissues analyzed (adrenal gland, breast, colon, liver and prostate). For all the state-of-the-art methods, a quantitative comparison was carried out by evaluating the relative square error (rSE) of the normalized image (global), nuclei and stroma (rSE_{global}, rSE_{nuclei} and rSE_{stroma}). Fig. 2 shows the comparison between SCAN and the state-of-the-art methods. The quantitative comparison showed that SCAN was the best method for stain normalization. Our technique obtained a rSE lower than 50% respect to the state-of-the-art methods [11–16].

The visual performances of the compared methods are reported in Fig. 3, where the results that contain typical artifacts are surrounded by an orange box. SCAN reported less image color artifacts than existing approaches due to its robustness (at estimating true stain vectors) and appropriateness (the physical meaning of concentration map was maintained in the estimate of matrix H). In fact, the approaches proposed by Vahadane et al. [15] and Khan et al. [13] failed in prostate and breast tissue slices, respec-

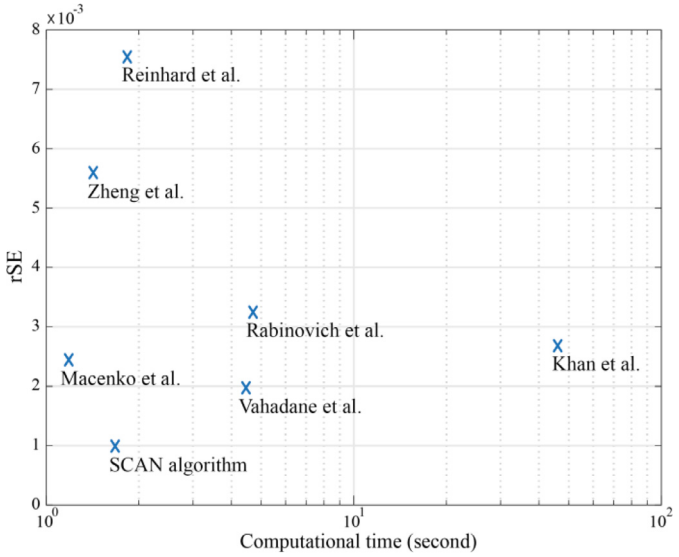

Fig. 4. Joint plot of rSE and average running time for computing the stain normalization, where the time is counted in second and presented in logarithmic coordinates.

tively, where the cellular structures were made darker respect to the target image. The high performances of our algorithm were mainly due to the combination of segmentation and classification techniques for rapid cellular structures segmentation. The useful pre-processing step of white detection, which was not based on a simple thresholding as in other works [11,16] allowed to adaptively detect the uncolored regions (e.g. background, gland lumen, etc.) which were removed from the analysis, with a consequent improvement of stain color estimation and normalization. The result of this strategy was highlighted (Fig. 3) especially for the liver tissue.

Table 3
Accuracy of a CNN model for breast cancer detection by varying the stain normalization method applied to the input images.

Normalization method	Accuracy	Precision	Recall	F1score
Original images	81.59%	79.78%	84.60%	82.12%
Macenko et al. [11]	88.41%	86.95%	90.40%	88.64%
Reinhard et al. [12]	82.98%	82.20%	84.20%	83.18%
Khan et al. et al. [13]	89.19%	87.68%	91.16%	89.39%
Rabinovich et al. [14]	88.67%	86.91%	91.03%	88.92%
Vahadane et al. [15]	90.56%	90.03%	91.23%	90.62%
Zheng et al. [16]	88.67%	87.68%	89.96%	88.81%
SCAN algorithm	**92.87%**	**92.33%**	**93.50%**	**92.91%**

The joint results of the quantitative metric (rSE) and running time of the compared methods are presented in Fig. 4. The processing was performed on a workstation with a 3.1 GHz quad-core CPU and 32 GB of RAM. For the SCAN algorithm, the average time of the stain normalization was 1.67 s, which is relatively low compared to other methods. The performance of the proposed method can be graphically represented as the point at minimum distance from the origin in the plane of stain normalization error (rSE) vs computational time. This means that our method is accurate and fast at the same time respect to state-of-the-art approaches.

In the last few years, deep neural networks drove advances in image recognition, and they achieved state-of-the-art performance in many fields of medical imaging [25]. Above all, convolutional neural networks (CNNs) have shown promising results in several classification and segmentation tasks [26]. Recent studies demonstrated the use of deep learning methods for computer-aided classification in H&E stained histopathological slices [27]. Hence, we have conducted experiments to evaluate the improvement of a CNN model using different methods of stain normalization. Specifically, a pre-trained AlexNet [28] was applied to the Camelyon-16 dataset (https://camelyon16.grand-challenge.org/) for breast cancer detection. The results obtained are summarized in Table 3. The SCAN algorithm was able to increase the quality of a computer-

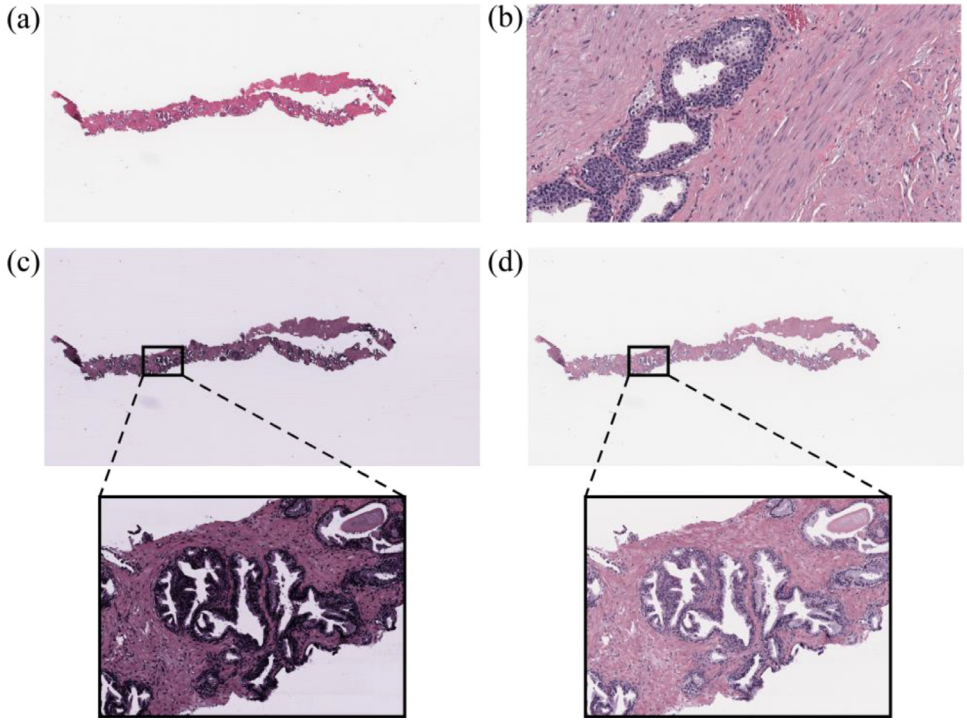

Fig. 5. Comparison in WSI normalization between the current state-of-the-art method and our algorithm. (a) original WSI, (b) target image, (c) stain normalization presented by Vahadane et al. [15], (d) stain normalization performed by SCAN.

aided diagnosis (CAD) system designed for cancer detection, improving the accuracy by more than 11% compared to the use of non-normalized images.

The method proposed by Vahadane et al. [15] obtained better results for the stain normalization process than other state-of-the-art methods and for this reason, we qualitatively compared the performance of WSI normalization between this method and our algorithm (Fig. 5). The model of Vahadane et al. [15] was solved by alternating between the stain color appearance matrix W and the stain density map H which optimized a well-defined cost function. However, the computational complexity of this method dramatically increased during the analysis of WSIs due to the large number of pixels. This leads to an exponential increase in computational time during the stain normalization: 247 s (Vahadane et al.) vs 37 s (the proposed). In addition, WSIs typically present a non-uniform and grayscale background, which becomes a color artifact during the normalization process, especially for iterative optimization-based methods [15,16] with a consequent worsening of stain normalization performances. The proposed method solves this problem with a pre-processing step of background detection in the preliminary stain estimation.

5. Conclusions

Color inconsistency between different scanners and laboratories is a significant issue in histopathology. Stain normalization is able to reduce the stain variability and improve the robustness of computer assisted diagnostic and image quantification algorithms. In this paper we present a novel algorithm (SCAN: Stain Color Adaptive Normalization) for rapid and accurate stain separation and normalization of histological slides. The proposed method was both quantitatively and qualitatively superior to the state-of-the-art techniques. Additionally, our method was reproducible (it was not based on different initializations of matrices W and H), adaptive (it was a refinement of the SVD-based approach [11]), robust (it was tested on a multiscale and multi-tissue dataset), light (it did not solve an optimization problem) and applicable to WSIs. The normalization of the proposed method is a pixel-wise transformation; hence it can be efficiently completed by parallel computing on CPU and GPU.

The limitations of the SCAN algorithm are related to the input image size and stain content: if the dimensions are too small or if one of the two stains (H&E) is not present in the image, the preliminary stain separation could fail because it is based on the method proposed by Macenko et al. [11]. In fact, if a stain binds to a few pixels of the image, the preliminary stain separation is not able to detect the specific stain and the entire normalization pipeline could consequently be involved with suboptimal results. In addition, the proposed method needs an image acquired with at least 5x magnification otherwise, with a lower resolution, the cellular structures segmentation may fail due to the poor quality of the image. For example, at 2x magnification (conversion factor: 4.67 μm/pixel) the cell nuclei are not visible and therefore they cannot be accurately segmented to estimate the hematoxylin concentration. However, in clinical practice this is not a problem because the digital histological slices are typically acquired with a magnification equal or higher than 10x [29].

The stain separation performed by SCAN is based on the Beer–Lambert law. Hence, our algorithm is potential to be applied to other stains that satisfy Beer–Lambert law (i.e. trichrome and giemsa stain, periodic acid–schiff stain, alcian blue stain). Future studies are required to test the performance of this method for the normalization of stains that do not follow the Beer–Lambert law (e.g. some immunohistochemical stains [30]). In the future, the SCAN algorithm could be integrated into deep learning frameworks to increase the performance of CNNs designed to segment or classify the cellular structures within the histological tissue. The proposed approach could also be implemented for other imaging modalities, such as fluorescence microscopy [31] or dermoscopy [32], in which the issue of intensity variation among different images has not yet been fully solved. Our research group is currently working on a more general stain separation approach, for extending the application scope of the proposed color normalization method. The importance of the stain normalization approach, proposed in this work, could be not only the improvement of clinical diagnosis in digital histopathology, but it could be a powerful pre-processing strategy to automated classification techniques for cancer detection tasks.

Declaration of Competing Interest

We declare that we do not have any commercial or associative interest that represents a conflict of interest in connection with the work submitted.

Acknowledgment

This study was supported in part by the institutional grant of the Proof of Concept of Politecnico di Torino (POC, Italy), Grant no. POC_16499. The authors would like to acknowledge Dr. Martino Bosco (Ospedale San Lazzaro, Turin, Italy) for his valuable assistance during the choice of optimal target images.

Supplementary materials

Supplementary material associated with this article can be found, in the online version, at doi:10.1016/j.cmpb.2020.105506.

References

[1] A.H. Fischer, K.A. Jacobson, J. Rose, R. Zeller, Hematoxylin and eosin staining of tissue and cell sections, CSH Protoc. 2008 (2008) pdb.prot4986, doi:10.1101/pdb.prot4986.
[2] M.N. Gurcan, L.E. Boucheron, A. Can, A. Madabhushi, N.M. Rajpoot, B. Yener, Histopathological image analysis: a review, IEEE Rev. Biomed. Eng. 2 (2009) 147–171, doi:10.1109/RBME.2009.2034865.
[3] A. Mouelhi, H. Rmili, J. Ben Ali, M. Sayadi, R. Doghri, K. Mrad, Fast unsupervised nuclear segmentation and classification scheme for automatic allred cancer scoring in immunohistochemical breast tissue images, Comput. Methods Progr. Biomed. 165 (2018) 37–51.
[4] S.G. Veloso, M.F. Lima, P.G. Salles, C.K. Berenstein, J.D. Scalon, E.A. Bambirra, Interobserver agreement of Gleason score and modified Gleason score in needle biopsy and in surgical specimen of prostate cancer, Int. Braz J. Urol. 33 (2007) 639–646 discussion 647-51, doi:10.1590/s1677-55382007000500005.
[5] T.T.E. Yeo, S.H. Ong, R. Sinniah, Autofocusing for tissue microscopy, Image Vis. Comput. 11 (1993) 629–639, doi:10.1016/0262-8856(93)90059-P.
[6] J.D. Bancroft, M. Gamble, Theory and practice of histological techniques, Elsevier Health Sciences, 2008, pp. 83–120.
[7] S. Hodgson, R.F. Harrison, S.S. Cross, An automated pattern recognition system for the quantification of inflammatory cells in hepatitis-C-infected liver biopsies, Image Vis. Comput. 24 (2006) 1025–1038, doi:10.1016/j.imavis.2006.02.019.
[8] M. Niethammer, D. Borland, J.S. Marron, J. Woosley, N.E. Thomas, Appearance normalization of histology slides, Int. Workshop Mach. Learn. Med. Imaging 6357 (2010) 58–66, doi:10.1007/978-3-642-15948-0_8.
[9] M. Salvi, F. Molinari, N. Dogliani, M. Bosco, Automatic discrimination of neoplastic epithelium and stromal response in breast carcinoma, Comput. Biol. Med. 110 (2019) 8–14, doi:10.1016/j.compbiomed.2019.05.009.
[10] J.T. Kwak, S.M. Hewitt, Multiview boosting digital pathology analysis of prostate cancer, Comput. Methods Progr. Biomed. 142 (2017) 91–99.
[11] M. Macenko, M. Niethammer, J.S. Marron, D. Borland, J.T. Woosley, X. Guan, C. Schmitt, N.E. Thomas, A method for normalizing histology slides for quantitative analysis, in: 2009 IEEE Int. Symp. Biomed. Imaging From Nano to Macro, 2009, pp. 1107–1110, doi:10.1109/ISBI.2009.5193250.
[12] E. Reinhard, M. Adhikhmin, B. Gooch, P. Shirley, Color transfer between images, IEEE Comput. Graph. Appl. 21 (2001) 34–41, doi:10.1109/38.946629.
[13] A.M. Khan, N. Rajpoot, D. Treanor, D. Magee, A nonlinear mapping approach to stain normalization in digital histopathology images using image-specific color deconvolution, IEEE Trans. Biomed. Eng. 61 (2014) 1729–1738, doi:10.1109/TBME.2014.2303294.

[14] A. Rabinovich, S. Agarwal, C. Laris, J.H. Price, S.J. Belongie, Unsupervised color decomposition of histologically stained tissue samples, in: S. Thrun, L.K. Saul, B. Schölkopf (Eds.), Adv. Neural Inf. Process. Syst., 16, MIT Press, 2004, pp. 667–674. http://papers.nips.cc/paper/2497-unsupervised-color-decomposition-of-histologically-stained-tissue-samples.pdf.

[15] A. Vahadane, T. Peng, A. Sethi, S. Albarqouni, L. Wang, M. Baust, K. Steiger, A.M. Schlitter, I. Esposito, N. Navab, Structure-Preserving color normalization and sparse stain separation for histological images, IEEE Trans. Med. Imaging 35 (2016) 1962–1971, doi:10.1109/TMI.2016.2529665.

[16] Y. Zheng, Z. Jiang, H. Zhang, F. Xie, J. Shi, C. Xue, Adaptive color deconvolution for histological WSI normalization, Comput. Methods Progr. Biomed. 170 (2019) 107–120, doi:10.1016/J.CMPB.2019.01.008.

[17] D.F. Swinehart, The Beer–Lambert law, J. Chem. Educ. 39 (1962) 333, doi:10.1021/ed039p333.

[18] C.M. van der Loos, Multiple immunoenzyme staining: methods and visualizations for the observation with spectral imaging, J. Histochem. Cytochem. 56 (2007) 313–328, doi:10.1369/jhc.2007.950170.

[19] M. Gavrilovic, J.C. Azar, J. Lindblad, C. Wählby, E. Bengtsson, C. Busch, I.B. Carlbom, Blind color decomposition of histological images, IEEE Trans. Med. Imaging 32 (2013) 983–994, doi:10.1109/TMI.2013.2239655.

[20] A.C. Ruifrok, D.A. Johnston, Quantification of histochemical staining by color deconvolution, Anal. Quant. Cytol. Histol. 23 (2001) 291–299.

[21] D.D. Lee, H.S. Seung, Algorithms for non-negative matrix factorization, in: Proc. 13th Int. Conf. Neural Inf. Process. Syst., MIT Press, Cambridge, MA, USA, 2000, pp. 535–541, doi:10.5555/3008751.3008829.

[22] S.E. Grigorescu, N. Petkov, P. Kruizinga, Comparison of texture features based on Gabor filters, IEEE Trans. Image Process. 11 (2002) 1160–1167, doi:10.1109/TIP.2002.804262.

[23] M. Salvi, F. Molinari, Multi-tissue and multi-scale approach for nuclei segmentation in H&E stained images, Biomed. Eng. Online 17 (2018) 89, doi:10.1186/s12938-018-0518-0.

[24] D. Arthur, S. Vassilvitskii, k-means++: the advantages of careful seeding, in: Proc. Eighteenth Annu. ACM-SIAM Symp. Discret. Algorithms, Society for Industrial and Applied Mathematics, 2007, pp. 1027–1035.

[25] T. He, H. Mao, J. Guo, Z. Yi, Cell tracking using deep neural networks with multi-task learning, Image Vis. Comput. 60 (2017) 142–153.

[26] J. Isaksson, I. Arvidsson, K. Åaström, A. Heyden, Semantic segmentation of microscopic images of H E stained prostatic tissue using CNN, in: 2017 Int. Jt. Conf. Neural Networks, 2017, pp. 1252–1256, doi:10.1109/IJCNN.2017.7965996.

[27] H. Sharma, N. Zerbe, I. Klempert, O. Hellwich, P. Hufnagl, Deep convolutional neural networks for automatic classification of gastric carcinoma using whole slide images in digital histopathology, Comput. Med. Imaging Graph. 61 (2017) 2–13, doi:10.1016/j.compmedimag.2017.06.001.

[28] H.-C. Shin, H.R. Roth, M. Gao, L. Lu, Z. Xu, I. Nogues, J. Yao, D. Mollura, R.M. Summers, Deep convolutional neural networks for computer-aided detection: CNN architectures, dataset characteristics and transfer learning, IEEE Trans. Med. Imaging 35 (2016) 1285–1298.

[29] A.D. Belsare, M.M. Mushrif, Histopathological image analysis using image processing techniques: an overview, Signal Image Process. 3 (2012) 23.

[30] T. Chen, C. Srinivas, Group sparsity model for stain unmixing in brightfield multiplex immunohistochemistry images, Comput. Med. Imaging Graph. 46 (2015) 30–39, doi:10.1016/j.compmedimag.2015.04.001.

[31] M. Salvi, U. Morbiducci, F. Amadeo, R. Santoro, F. Angelini, I. Chimenti, D. Massai, E. Messina, A. Giacomello, M. Pesce, F. Molinari, Automated segmentation of fluorescence microscopy images for 3D cell detection in human-derived cardiospheres, Sci. Rep. 9 (2019) 6644, doi:10.1038/s41598-019-43137-2.

[32] C. Barata, M.E. Celebi, J.S. Marques, Improving dermoscopy image classification using color constancy, IEEE J. Biomed. Heal. Inform. 19 (2014) 1146–1152.